Nucleation of NaCl Nanoparticles in Supercritical Water: Molecular Dynamics Simulations

ARTICLE *in* THE JOURNAL OF PHYSICAL CHEMISTRY B · JULY 2008

Impact Factor: 3.3 · DOI: 10.1021/jp709688g · Source: PubMed

3 AUTHORS, INCLUDING:

Istok Nahtigal
Bioniche Life Sciences Inc.
6 PUBLICATIONS **61** CITATIONS
SEE PROFILE

Igor M. Svishchev
Trent University
70 PUBLICATIONS **1,855** CITATIONS
SEE PROFILE

Nucleation of NaCl Nanoparticles in Supercritical Water: Molecular Dynamics Simulations

Istok G. Nahtigal, Alexander Y. Zasetsky, and Igor M. Svishchev*

Department of Chemistry, Trent University, Peterborough, Ontario, Canada K9J 7B8

Received: October 3, 2007; Revised Manuscript Received: April 16, 2008

Formation of NaCl nanoparticles in supercritical water is studied using molecular dynamics simulation method. We have simulated particle nucleation and growth in NaCl−H_2O fluids, with salt concentration of 5.1 wt %, in the temperature and density range of 673−1073 K and 0.17−0.34 g/cm^3, respectively. The cluster size distributions, the size of critical nuclei and cluster lifetimes are reported. The size distribution of emerging clusters shows a very strong dependence on the system's density, with larger clusters forming at lower densities. Clusters consisting of approximately 14−24 ions appear critical for the thermodynamic states examined. The local structures of critical clusters are found to be amorphous. The lifetime values for clusters containing more than 20 ions are in the range of 10−50 ps. We have calculated the NaCl nucleation rates, which appear to be on the order of 10^{28} cm^{-3} s^{-1}.

I. Introduction

High-temperature water is used in many traditional and modern technologies like power generation, hazardous waste extraction and utilization, and materials processing. Precipitation of solid salt particles often causes serious problems in hydrothermal applications, where metastable steam or supercritical fluids are employed. For example, the thermodynamic conditions in the moisture transition region in power turbines are able to activate the mechanism of nucleation and growth of liquid droplets composed of concentrated salt solutions.[1,2] These salt solutions provide the basis for the nucleation of solid salt particles, which in turn promote a significantly higher frequency of corrosion events within this region. The processes in supercritical water oxidation (SCWO) reactors are also affected by the presence of such solid particles, which may salt out from a solution in the supercritical region and thus have serious ramifications on the process efficiency and safety.[3] Sodium chloride is certainly a major chemical species in these processes. An equilibrium phase diagram for the NaCl−H_2O system is now thought to be well characterized in the range of temperatures and pressures.[4–6] The formation of solid salt particles is, however, a kinetic process taking place in a metastable state of a system and is as yet not completely understood.

First-order phase transitions such as crystallization proceed through the nucleation and growth of critical embryos (by monomer deposition and cluster−cluster coalescence).[7,8] The nucleation process requires some impetus, usually in the form of spontaneous density or composition fluctuations within the metastable phase.[8] An energy cost is associated with the creation of a new phase; the penalty is the interface energy, which diminishes as the clusters' surface to volume ratio decreases. In a metastable system this leads to the existence of a critical size, beyond which growth is favored. The critical-sized nucleus, or embryo, need not possess the properties of the stable thermodynamically phase, but one that is closest in free energy to the parent phase.[8,9]

In an aqueous environment the number density ratio of solute to solvent species is typically small, with the solvent maintaining thermal equilibrium. Ions interact as solvent-separated species, partial dehydration of the ions results in the formation of contact pairs, which then evolve into a cluster. Solvated clusters tend to have both crystal-like and liquidlike (amorphouslike) orders. An embryo which grows to a size larger than the critical size, will most likely continue to grow to a macroscopic size, whereas ones smaller than critical will likely reduce in size.[10,11] From a kinetic viewpoint, a critical embryo can be considered as a transient species appearing and disappearing at some steady rate specific to the thermodynamic conditions.

TABLE 1: Lennard-Jones Interaction Parameters and Site Charges from Smith and Dang[16]

element	ϵ (kJ/mol)	σ (nm)	q (eps)
Na^+	0.54431	0.2350	1.0000
Cl^-	0.41870	0.4400	−1.0000
O	0.65000	0.3166	−0.8476
H	0.00000	0.0000	0.4238

The nucleation dynamics and cluster structures can be directly examined by using molecular dynamics (MD) simulations. MD method provides crucial microscopic insights into the processes of nucleation and particle growth; it also enables one to calculate the nucleation rate, the macroscopic quantity that is difficult to measure experimentally.[13] The kinetics of the initial stages of NaCl cluster formation in SCW have been recently[12] examined for three state points of low density (0.1−0.14 g/cm^3) and high salt concentration (20.2 wt %). It is the purpose of this paper to investigate the nucleation of NaCl nanoparticles in a wider range of density and temperature from the trajectories generated by the MD method. We explore the NaCl−H_2O system at a lower salt concentration (5.1 wt %), which is useful for providing direct insights into the particle formation kinetics in the hydrothermal equipment.

II. Computational Methodology

A. Simulation Details. In the present work we have employed a parallel molecular dynamics code for an arbitrary molecular mixture (M.DynaMix) by Lyubartsev and Laaksonen,[14] modified to perform the clustering analysis. The simple point charge extended (SPC/E) model was used for water.[15] The SPC/E model provides a reasonably good prediction of the

* To whom correspondence should be addressed. Phone: 705-748-1011 ext. 7063. Fax: 705-748-1625. E-mail: isvishchev@trentu.ca.

10.1021/jp709688g CCC: $40.75
Published on Web 05/31/2008

TABLE 2: Details of MD Simulations and Statistics for Largest NaCl Clusters

T (K)	density (g/cm^3)	H_2O	Na^+	Cl^-	simulation time (ns)	largest cluster (atoms)	lifetime of largest cluster (ps)
673	0.17	4000	66	66	1.0	108	200
873	0.17	4000	66	66	1.0	112	12
1073	0.17	4000	66	66	1.0	122	16
673	0.25	4000	66	66	1.0	60	6
873	0.25	4000	66	66	1.0	40	22
1073	0.25	4000	66	66	1.0	35	3
673	0.34	4000	66	66	1.0	46	6
873	0.34	4000	66	66	1.0	40	8
1073	0.34	4000	66	66	1.0	44	7

structure and dielectric constant for water. The calculated values for the dielectric constant are, approximately, 81 at 298 K and 6 at T_C, as compared with 78.0 and 5.3, respectively, for real water. We have also employed Smith and Dang's parameters[16] to model ion−ion and ion−water interactions, as they have been optimized for use with the SPC/E water model. Table 1 lists site charges, q, and Lennard-Jones parameters, ϵ and σ. The Lorentz−Berthelot mixing rules were applied for cross terms

$$\sigma_{ij} = \frac{\sigma_i + \sigma_j}{2} \tag{1}$$

and

$$\varepsilon_{ij} = \sqrt{\varepsilon_i \varepsilon_j}$$

The equations of motion were solved by using Verlet leapfrog algorithm, with the time step of 2 fs. The SHAKE constraints scheme[17] was applied to keep molecules rigid. Simulations have been performed in the NVT ensemble (isochoric−isothermal conditions) with temperature controlled by the Nosé−Hoover thermostat.[18]

We have employed the reaction field (RF) periodic boundary conditions using cubic geometry for the basic simulation cell. "Conducting" boundary was assumed with the RF cutoff radius being set at 2.5 nm. We have also performed a test run at the density of 0.34 g/cm^3 and temperature of 673 K using the Ewald method. The total energy calculated using Ewald sums was found to be −24.57 kJ/mol, while the RF method yields −24.39 kJ/mol. Note that the energy difference is within the sampling (statistical) error (of about 1.5%). The average pressure values calculated with both methods were also very similar.

In each simulation 4000 water molecules were initially equilibrated at the temperature of interest. Then, 132 ions were randomly distributed over the simulation cell in such a way to prevent the formation of any contact ion-pairs at the beginning and the overlap with water molecules. Following ion insertion, the trajectories of atoms were sampled without further equilibration. The solution concentration was 5.1 wt % of NaCl. The system size, production run lengths, temperatures, and solution densities are as specified in Table 2. The ion clustering was surveyed by assigning a specific connection (link) between neighboring ions. In this study the following definition of a cluster is used: (a) any two adjacent atoms are connected if they are separated by a distance less than 0.42 nm (which corresponds to the average between the first minima in the Na^+-Na^+, $Na-Cl^-$ and Cl^--Cl^- radial distribution functions in NaCl melts[19]) and (b) any two atoms belong to the same cluster if there is a continuous path connecting them. The clusters have been sampled at each and every hundredth step during the production runs with the clustering analysis being performed on the fly.

TABLE 3: Nucleation Rates and Critical Nucleus Sizes

T (K)	density (g/cm^3)	critical nucleus N[a] (atoms)	induction period τ_c (ps)	nucleation rate J ($\times 10^{28}$ cm^{-3} s^{-1})
673	0.17	22−24	55	1.19
873	0.17	17−19	70	1.83
1073	0.17	24	75	3.82
673	0.25	18	81	1.36
873	0.25	18	90	2.08
1073	0.25	21	108	3.91
673	0.34	14−16	98	1.55
873	0.34	16	111	2.15
1073	0.34	16	130	3.96

[a] Critical sizes yielding constant nucleation rate.

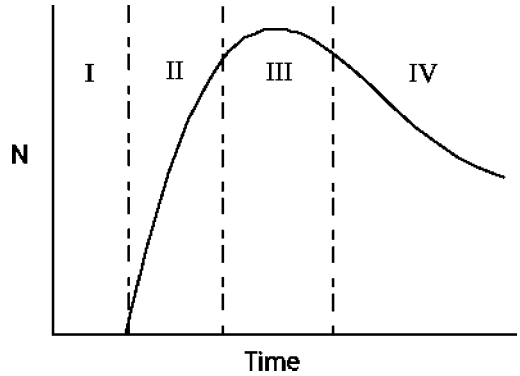

Figure 1. Typical growth−decay evolution curve for the number of nuclei (N) larger than a threshold size. Domain I, the induction period where no nuclei larger than critical are observed; domain II, the nucleation regime; domain III, the generation of nuclei stops; domain IV, the coarsening regime.

B. Nucleation Rate. The nucleation rate J is defined as the number of nuclei larger than the critical size generated per unit volume per unit time. We have estimated the nucleation rate by using a kinetic approach of Yasuoka and Matsumoto.[20] The number of clusters above a certain threshold size is counted and plotted against time, producing a growth−decay evolution curve shown schematically in Figure 1. The size of the critical nucleus can be estimated from the slope of the growth curve. With increasing threshold size, the inclination of the growth curve (domain II in Figure 1) decreases, at the critical size the inclination stops decreasing (and remains constant for larger threshold sizes). From a kinetic perspective this is where growth and decay are balanced, yielding the size of the critical nucleus. The nucleation rate J is, specifically, the slope of the evolution curve for the cluster sizes above critical, normalized to the volume of the simulation cell. Note that there is a finite induction time before the system reaches a metastable equilibrium[21] and no nuclei larger than the critical are observed (domain I in Figure 1). This induction (lag) time is also reported here.

At the theoretical level, it is extremely difficult to quantitatively describe the nucleation process using the classical nucleation theory (CNT).[22] Within the framework of the CNT, the total (Gibbs) free energy of the formation of a new phase nucleus is a combination of the energy "gain" for transforming unit volume of the system to the new phase and the energy "loss" due to the interface formation. The difficulties in applying the CNT approach to a real multicomponent system result primarily from an inadequate account of the interface effect. Real interfaces may have a complex density profile, markedly nonuniform structure and composition. In our case, an accurate knowledge of the high-temperature thermodynamics of electrolyte solutions is also required.

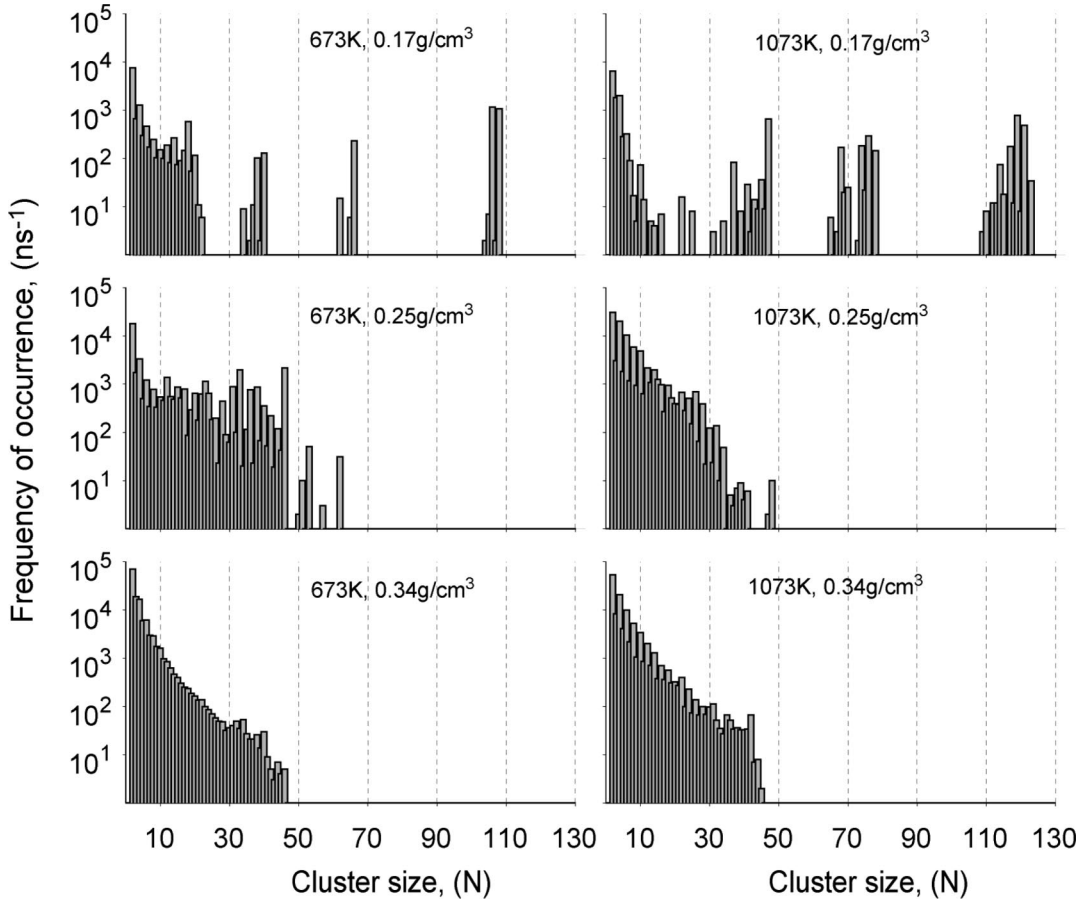

Figure 2. Cluster size distributions (frequency of occurrence of the clusters of different size) for the final 0.7 ns of the simulation trajectory.

C. Size and Structure. To probe the internal structure of NaCl clusters, the local order parameter q_l, as described by ten Wolde et al.,[23,24] is used. We have chosen to work with the fourth-order symmetry parameter, q_4, as it is most suited for the analysis of cubic close packing (NaCl solid structure);[25] higher orders of symmetry would be redundant. In the recent work by Valeriani et al.[25] the q_4 parameter has been successfully employed to analyze the degree of crystallinity in molten sodium chloride.

In a simulation, the normalized parameter $q_4(i)$ for each atom in a cluster is first calculated by

$$\mathbf{q}_{4m}(i) = \frac{\frac{1}{N(i)}\sum_{j=1}^{N}\mathbf{Y}_{4m}(\mathbf{r}_{ij})}{||\mathbf{q}_{4m}(i)||} \tag{2}$$

where $Y_{lm}(\mathbf{r}_{ij})$ is the angular component of the spherical harmonics, $N(i)$ is the number of adjacent atoms that lie within the first minimum of the Na^+-Cl^- radial distribution function, and $\mathbf{r}_{ij}$ is the unit vector that indicates the direction of bond between a central particle i and its neighbors j. Then, the value of a scalar product q_4 for neighboring particles i and j is computed by

$$q_4(i)q_4^*(j) = \sum_{m=-4}^{4}\mathbf{q}_{4m}(i)\mathbf{q}_{4m}^*(j) \tag{3}$$

Finally, following the work of Valeriani et al.,[25] we compile a histogram of a number of crystal-like connections (a number of scalar products of particle i with neighboring particles in which the value of $q_4(i)$ exceeds 0.35), using all the atoms in a particular cluster. This histogram represents the probability for an ion in this cluster to possess a certain number of crystal-like connections.[24] Note that ions linked by a crystal-like connection can be present in amorphous clusters; only those ions that possess 6 or more of such connections are considered as being in a crystalline environment. In other words, the local NaCl structure can be considered crystalline if its q_4 value is greater than or equal to 6. In this work, we compare the q_4 histogram for NaCl clusters against the q_4 parameter distribution for an ideal NaCl crystal, which helps determine whether the simulated nanoparticles are amorphous or crystalline.

To investigate the compactness of our clusters we calculate the hydrodynamic (R_{hyd}) and gyration (R_g) radii distributions,[26] which are also known to be highly dependent on the order in the cluster. In this work R_g and R_{hyd} are computed by the following means

$$R_{hyd} = \left[\frac{1}{N^2}\sum_{ij}\frac{1}{R_{ij}}\right]^{-1} \tag{4}$$

$$R_g = \frac{1}{N}\sqrt{\frac{1}{2}\sum_{ij}R_{ij}^2} \tag{5}$$

where R_{ij} is the separation between ions i and j and N is the number of ions making up the cluster.

III. Results and Discussion

In this work we examine the kinetics of formation and growth of NaCl particles, from random ion arrangements, in samples of supercritical water at temperatures of 673, 873, and 1073 K and densities of 0.17, 0.25, and 0.34 g/cm^3. We identify critical

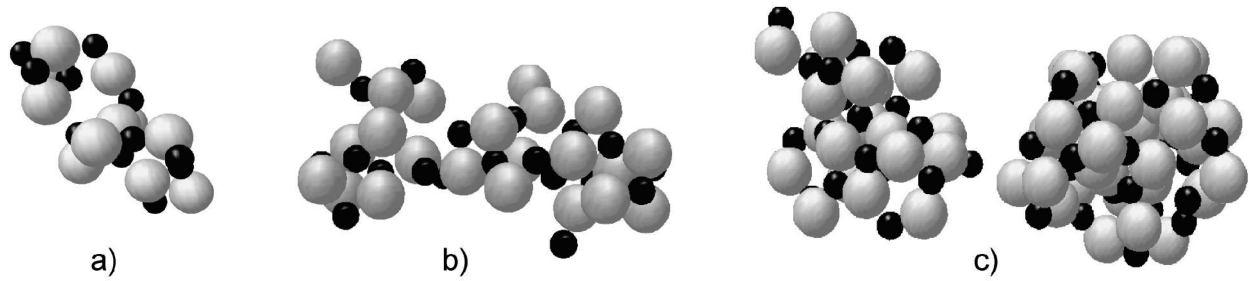

Figure 3. Evolution of clusters at 673 K and 0.17 g/cm^3. (a) Typical near-critical size cluster (20 ions), (b) fusion of 2 critical nuclei (25 and 22 ions) into larger postcritical particle, and (c) condensation of two postcritical particles. Large spheres are chloride ions, small spheres are sodium ions.

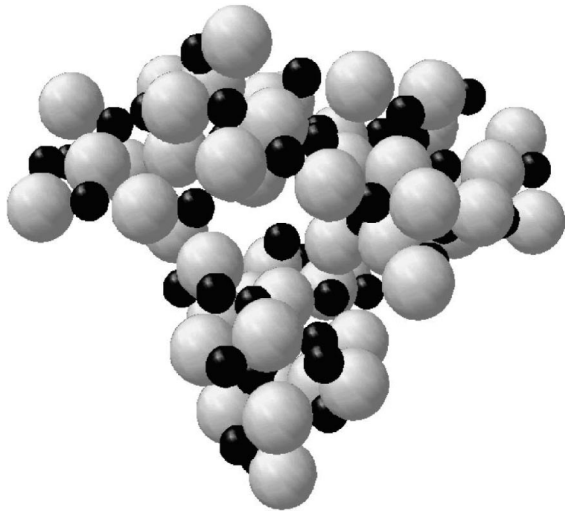

Figure 4. Example of a postcritical amorphous NaCl particle composed of 112 atoms formed by condensation of smaller clusters at 1073 K and 0.17 g/cm^3.

size clusters, examine their local structure, and estimate the NaCl nucleation rate. Note that the equilibrium high-temperature phases[3] for the chosen composition and densities are liquid solutions at 673 K (close to solid−vapor phase separation), coexisting solid and vapor at 873 K and coexisting vapor and liquid at 1073 K.

Figure 2 displays cluster size distributions generated at different state points. These distributions are normalized by the length of the analyzed trajectory, thereby representing the frequency of occurrence of clusters of different sizes. The most obvious result emerging from Figure 2 is that cluster size distributions are strongly density dependent. Thus, for the solution with the density of 0.17 g/cm^3 the largest clusters observed during the course of simulation runs were 108 atoms at 673 K and 122 atoms at 1073 K, whereas for the solution with the density of 0.34 g/cm^3 clusters could only reach the size of 46 atoms at 673 K and 44 atoms at 1073 K. The temperature effect is less pronounced and, perhaps, larger systems and longer simulation times are required to assess the temperature effects on the cluster size distribution in more detail. We observe that at the lowest density, of 0.17 g/cm^3, large clusters tend to form faster at a high temperature of 1073 K, while for the solutions with the density of 0.34 g/cm^3 the distributions are rather similar for all the temperatures examined. It is also worthwhile noting that large clusters tend to form by coagulation of smaller clusters, especially at the lower density, which is an indication that two or more critical nuclei form independent of each other. The formation of many small clusters is kinetically favored (as they initially nucleate more easily), yet larger particles are more thermodynamically stable, and they eventually scavenge smaller clusters.

Figure 3 is the trajectory visualization for a system at the lowest density (0.17 g/cm^3) and temperature (673 K) that shows the process of the coagulation of smaller clusters (on the order of 20 atoms) into larger particles. In reference back to Figure 2 (in which the top panels reflect this coagulation process from a statistical viewpoint) we point to the gaps between peaks in the size distributions. These gaps indicate that once clusters reach the size of about 20 atoms the consequent growth progresses by the coagulation. This size (around 20) visually appears to be critical in the nucleation dynamics. For the 0.34 g/cm^3 solution, this critical size appears to be around 16 ions, with the growth and dissolution processes occurring more rapidly. The ion−water system at a higher density is more "liquidlike", and salt particles tend to be smaller and form (and dissolve) more readily.

A simple visual inspection of ionic configurations reveals that the emerging NaCl particles are amorphous. In fact, no crystalline arrangements resembling regular NaCl structure have been observed on the time-scale of our simulations, even for the largest particles. Figure 4 shows a postcritical amorphous NaCl cluster composed of 112 atoms, formed by the condensation of smaller clusters at the solution density of 0.17 g/cm^3 and temperature of 1073 K. By following the trajectories of individual clusters, we have observed that this and other large particles may split back into smaller fragments, or may eventually reorganize and become compact. Presumably, much larger systems and longer simulations will be needed to examine the coagulation of postcritical amorphous clusters into larger crystalline chunks of a solid material at supercritical conditions.

We now turn our attention to the calculation of the nucleation rates. Parts a−d of Figure 5 displays time dependence of the concentration of clusters of different sizes (growth−decay dynamics) at the density of 0.17 g/cm^3 and temperature of 673 K. The threshold sizes are 16, 20, 22, and 24; each point represents block-average over 50 ps. These figures clearly show the induction period before which no nuclei larger than the threshold size are observed. The thin solid line represents the slope of the growth curve. The nucleation rate can be calculated from the slope of the growth curve in parts c and d of Figures 5, which is constant at 1.19×10^{28} cm^{-3} s^{-1}, threshold sizes being 22 and 24, respectively. We thus assume that clusters of the size 22−24 appear critical for the nucleation dynamics at this state point. After about 0.25 ns, as the supersaturation gradually decreases, the concentration of clusters begins to plateau indicating stop in the generation of new nuclei. Another observation from Figure 5 is that postcritical nuclei tend to form by cluster−cluster fusions (rather than by gradual monomer

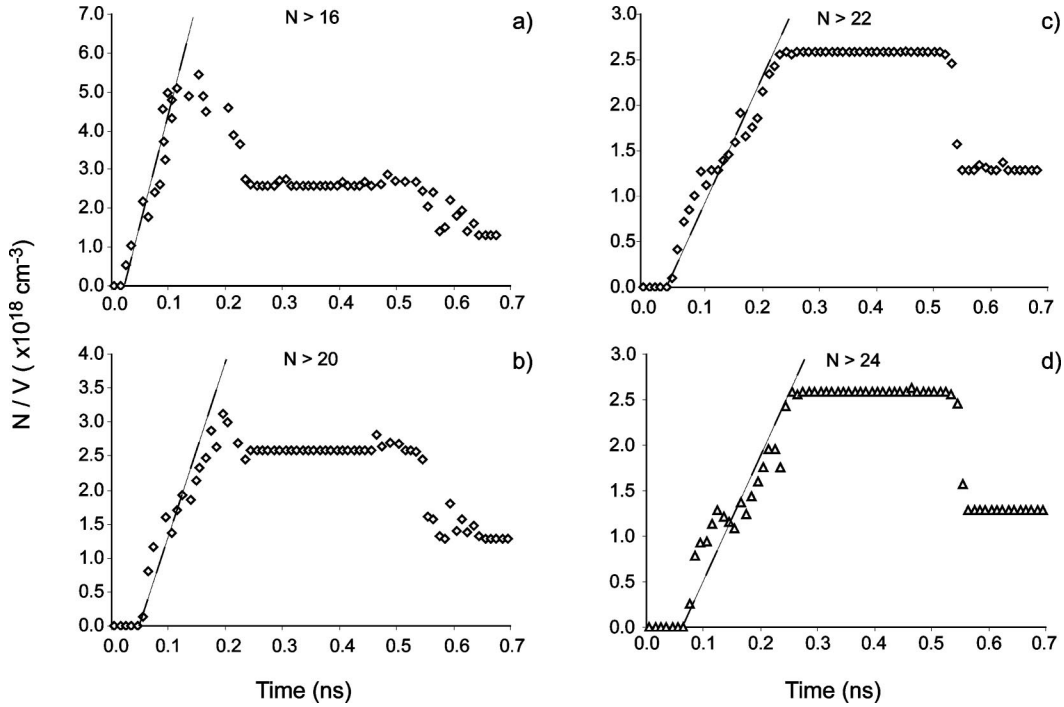

Figure 5. Time dependence of the concentration (N/V) of clusters larger than a threshold size (growth-decay evolution) in the 673 K and 0.17 g/cm^3 system. Threshold sizes are (a) 16, (b) 20, (c) 22, and (d) 24 ions; each point represents block-average over 50 ps. The thin solid line reflects the slope of the growth curve. In (c) and (d) the nucleation rate stops decreasing, remaining constant at 1.19×10^{28} cm^{-3}s^{-1}, for thresholds above $N = 22$.

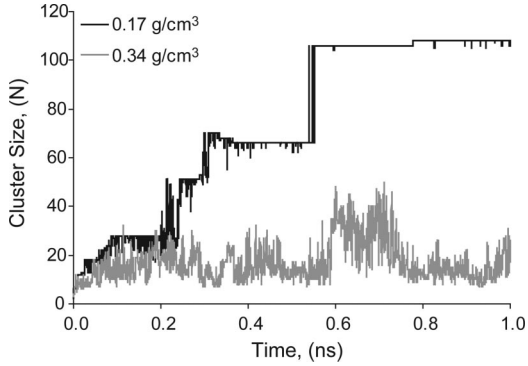

Figure 6. Cluster size evolution with time at 673 K for high (the black line) and low (the gray line) densities.

addition), as illustrated by the stepwise decay of the cluster distributions at times larger than 0.5 ns.

All nucleation rates calculated are given in Table 2. They are, generally, on the order of 10^{28} cm^{-3} s^{-1} indicating very fast nucleation dynamics. The critical cluster sizes are also given, together with the induction (lag) period for the critical cluster, τ_c. On the whole, the nucleation rate increases modestly with the increase in temperature and density, and the critical size tends to be larger at the lower density.

Cluster lifetimes were obtained by monitoring the evolution of cluster sizes with time. Figure 6 shows a temporal evolution of cluster sizes for two states at 673 K, one at the density of 0.17 g/cm^3 and another at 0.34 g/cm^3. Cluster size values in Figure 6 are averaged within the bins of 5−9, 10−14, and 15−19 atoms and so forth (block-averaged). The cluster lifetime values are obtained by measuring the length of continuous horizontal lines in Figure 6. In other words, we assume that a certain particle continuously exists as long as the fluctuation in its size does not exceed the bin size (±2 atoms). The typical lifetime distributions are shown in Figure 7. The sizes and

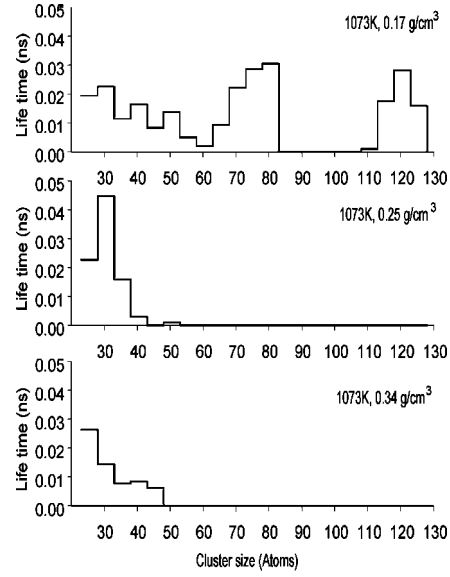

Figure 7. Lifetimes of NaCl clusters as a function of their size at 1073 K.

lifetimes of the largest clusters observed at a particular state point are included in Table 2. As can be seen in Figure 7, the average lifetime values for the clusters larger than 20 atoms are in the range between 10 and 50 ps. These rather short lifetimes observed for polyatomic clusters are comparable with the collision time between individual ions and smaller clusters.

The q_4 probability distribution for clusters formed at the density of 0.34 g/cm^3 and temperature of 673 K is shown in Figure 8. Similar histograms were obtained for other state points. The q_4 distribution peaks around 2. This indicates that emerging clusters are amorphous (or liquidlike). The q_4 parameter distribution for an ideal NaCl crystal is also shown in this figure to illustrate that there is no similarity between the simulated and ideal (solidlike) NaCl structures.

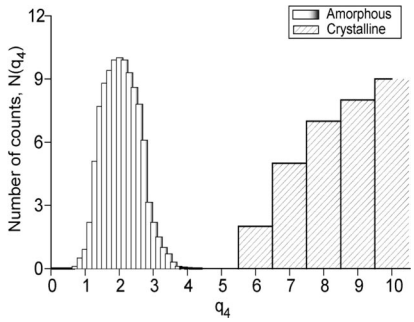

Figure 8. Order parameter distribution $N(q_4)$ for NaCl clusters at 1073 K and 0.17 g/cm^3; the histogram for crystalline NaCl sample is shown as a reference.

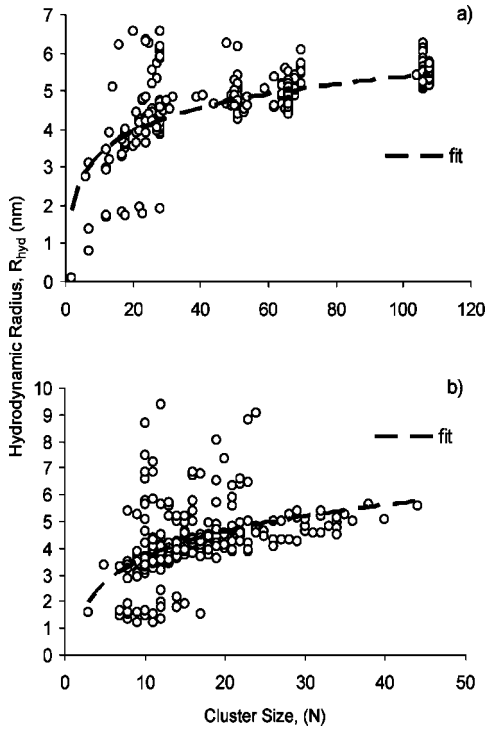

Figure 9. Hydrodynamic radii at (a) 673 K and 0.17 g/cm^3, (b) 673 K and 0.34 g/cm.^{3} Superimposed are logarithmic fitting curves of the form $R_{hyd} = k_1 \ln(N) + k_2$, where k_1 and k_2 are fitting parameters.

Hydrodynamic and gyration radii are presented, respectively, in Figures 9 and 10, as a function of the cluster size. As can be seen in these figures, the dispersion in the size of particles, especially around critical values (15−25), is large indicating that critical clusters can take on a wide variety of shapes. Larger clusters (postcritical nuclei) tend to take on more compact shapes and, as a result, show a smaller variation in the hydrodynamic radius value. The hydrodynamic radii appear to converge to about 5 nm for the systems studied in the present work. The radii of gyration show a similar trend. Also shown in Figure 9 is the logarithmic fit for the hydrodynamic radius as a function of the cluster size. In the close, we note that although cluster geometries vary substantially, the ion−ion separations in the larger clusters approach on average their crystal-like values. For example, the Na^+-Cl^- separations of about 0.285 nm (equilibrium bond length found in NaCl crystals) are found for clusters with N approaching 30. Presumably, these and larger clusters will have the potential to exhibit crystalline character in their physical properties and, eventually, crystallize.

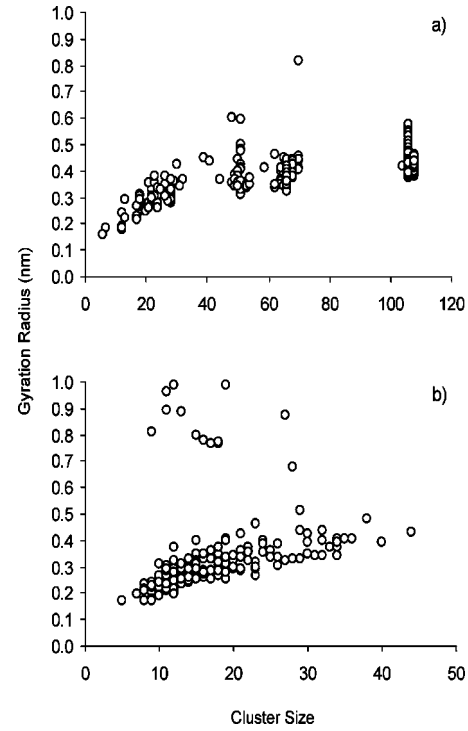

Figure 10. Gyration radii at (a) 673 K and 0.17 g/cm^3, (b) 673 K and 0.34 g/cm.^{3} Note that the upper and lower data groupings in part b give indication that clusters of near critical sizes may exist in two forms, diffuse and compact.

IV. Conclusions

Using MD simulations we have investigated the kinetics of formation and growth of sodium chloride clusters in supercritical water over wide range of state conditions. The cluster size distributions, the size of critical nuclei, and cluster lifetimes are reported. The size distribution of emerging clusters shows a very strong dependence on the system's density, with larger clusters formed at lower densities. The clusters consisting of approximately 14−24 ions appear critical for the thermodynamic states examined. The cluster−cluster fusion events seem to be important in the formation of larger particles, particularly at low densities. The lifetime values for clusters containing more than 20 ions are found to be on the order of 10 ps. We have calculated the NaCl nucleation rates, which appear to be on the order of 10^{28} cm^{-3} s^{-1}. We have also probed the degree of local order in emerging clusters, and it appears to be amorphous. Whereas this simulation work provides molecular-level insights into the crucial nucleation events, further studies using larger samples are necessary in order to provide a direct comparison with experimental data on nucleation[5,27] and to observe the formation of regular crystalline particles.

Acknowledgment. We are grateful for the financial support of the Natural Sciences and Engineering Research Council of Canada and SHARCNET. SHARCNET (www.sharcnet.ca) is a consortium of universities and colleges operating a network of high-performance computer clusters across southwestern, central, and northern Ontario.

References and Notes

(1) Bellows, J. C. In *Water, Steam and Aqueous Solutions for Electric Power*; Nakahara, M., Matubayasi, N., Ueno, M., Yasuoka, K., Watanabe, K. Eds.; Maruzen Co. Ltd.: Tokyo, 2005; p 612.

(2) Galobardes, J. F.; Van Hare, D. R.; Rogers, L. B. *J. Chem. Eng. Data* **1981**, *26*, 363.

(3) Hong, G. T.; Armellini, F. J.; Tester, J. W. In *Physical Chemistry of Aqueous Systems*; White, H. J., Jr., Sengers, J. V., Neumann D. B., Bellows, J. C. Eds.; Begell House: New York, 1994; p 565.
(4) Pitzer, K. S. *Int. J. Thermophys.* **1998**, *19*, 2.
(5) Armellini, F. J.; Tester, J. W. *J. Supercrit. Fluids* **1991**, *4*, 254.
(6) Bischoff, J. L. *Am. J. Sci.* **1991**, *291*, 309.
(7) Maksimov, I. L. *Crystallogr. Rep.* **2002**, *47*, 105.
(8) Debenedetti, P. G. In *Metastable Liquids: Concept and Principles*; Princeton Press: NJ, 1996.
(9) Ostwald, W. *Z. Phys. Chem.* **1897**, *22*, 289.
(10) Katz, J. L. *Pure Appl. Chem.* **1992**, *64*, 1661.
(11) Mokross, B. J. *J. Non-Cryst. Solids* **2001**, *284*, 91.
(12) Lummen, N.; Kvamme, B. *Phys. Chem. Chem. Phys.* **2007**, *9* (25), 3251.
(13) Gasser, U.; Weeks, E. R.; Schofield, A.; Pusey, P. N.; Weitz, D. A. *Science* **2001**, *292*, 258.
(14) Lyubartsev, A. P.; Laaksonen, A. *Comput. Phys. Commun.* **2000**, *128*, 565.
(15) Berendsen, H. J. C.; Grigera, J. R.; Straatsma, T. P. *J. Phys. Chem.* **1987**, *91*, 6269.
(16) Smith, D. E.; Dang, L. X. *J. Chem. Phys.* **1994**, *100*, 3757.
(17) Ryckaert, J. P.; Ciccotti, G.; Berendsen, H. J. C. *J. Comput. Phys.* **1977**, *23*, 327.
(18) Nosé, S. *Mol. Phys.* **1984**, *52*, 255.
(19) Lyubartsev, A. P.; Laaksonen, A. *J. Phys. Chem.* **1996**, *100*, 16410.
(20) Yasuoka, K.; Matsumoto, M. *J. Chem. Phys.* **1998**, *109*, 8451.
(21) Wang, H.; et al. *Phys. Rev. E* **2007**, *76*, 041116.
(22) Huitema, H. E. A.; van der Eerden, J. P.; Janssen, J. J. M.; Human, H. *Phys. Rev. B.* **2000**, *62*, 14690.
(23) ten Wolde, P. R.; Ruiz-Montero, M. J.; Frenkel, D. *J. Chem. Phys.* **1999**, *110*, 1591.
(24) ten Wolde, P. R.; Ruiz-Montero, M. J.; Frenkel, D. *J. Chem. Phys.* **1996**, *104*, 9932.
(25) Valeriani, C.; Sanz, E.; Frenkel, D. *J. Chem. Phys.* **2005**, *122*, 194501.
(26) Grosberg, A. Y.; Khokhlov, A. R. In *Statistical Physics of Macromolecules*; Atanov, Y. A. Ed.; AIP Press: New York, 1994.
(27) Strey, R.; Wagner, P. E.; Viisanen, Y. *J. Phys. Chem.* **1994**, *98*, 7748.

JP709688G